KSCE Journal of Civil Engineering (2018) 22(2):603-612
DOI 10.1007/s12205-017-1313-3

Hydraulic Engineering
pISSN 1226-7988, eISSN 1976-3808
www.springer.com/12205

Numerical Investigation on the Effect of Sudden Contraction on Flow Behavior in a 90-Degree Bend

Rasoul Daneshfaraz*, Ali Rezazadehjoudi, and John Abraham*****

Received July 29, 2016/Accepted March 19, 2017/Published Online June 23, 2017

Abstract

Here we investigate fluid flow in 90-degree bends with and without orifice-like constrictions. The results of flow in non-constricted bends were compared with experimental results for similar Reynolds numbers and found to be in good agreement. Calculations were then carried out for various Reynolds numbers in the laminar and turbulent regimes. In addition, constrictions up to a 60% blockage were incorporated. The present study shows that the Reynolds number and the presence of an orifice-like constriction affects the velocity profile and the pressure distribution. The results indicate that if a sudden contraction is encountered, the peak velocity is larger and the flow is more predisposed to the outer wall than it otherwise would be. In addition, a sudden contraction increases the pressure loss compared to the constant-area bend and it affects the pressure distribution throughout the entire bend. This paper provides a means to predict pressure losses (similar to minor loss coefficients) in rounded bends in the presence or absence of constrictions. Such information is important to practicing engineers for designing fluid-flow conveyance systems. The behavior of the fluid is shown to be connected to the constriction and is also affected by the Reynolds number.

Keywords: *numerical simulation, pressure drop, relative pressure drop, sudden contraction, velocity profile, bend*

1. Introduction

Bends and curves in pipes and ducts are commonly encountered in practical hydraulic situations and other fluid conveyance systems. In addition, sudden constrictions are common and are often found in the presence of pipe bends and curves. The constrictions may be unintentional or may be a purposeful part of the pipe-system design.

Some engineering applications where pipe bends are found include petrochemical, food processing, HVAC applications, medical devices, manufacturing, and other industries.

Basic theoretical, experimental, and numerical studies give clear expectations that constrictions present an added loss to the energy and pressure in a flow system. However quantifying the impact is a challenge. Analytical solutions in this case are virtually impossible. The alternative of experimentation is a possible investigation avenue however the multiple geometric parameters makes the cost and time prohibitive. Because of these limitations, numerical simulation will be used. This approach is becoming routine in fluid-flow studies for a variety of flow situations. For instance, Bovendeerd *et al*. (1978) investigated profile and contour of velocity in a 90 degree bend using the finite element method. They implemented a laminar parabolic velocity profile as an inlet condition and they provided a detailed description of the flow throughout the entire bend including the secondary motion and variations of axial velocity profiles at various streamwise locations. Another study (Van De Vosse, 1989) modeled a three-dimensional 90-degree bend using the finite element method and compared the numerical calculations with experiments of Olsen (1971). The comparison showed very good agreement between the simulations and experiments. Morrissey and Chouet (1997) used numerical simulation to calculate choked-flow dynamics and their role in triggering long-period events at Redoubt Volcano, Alaska.

More recently, Al-Qahtani *et al*. (2002) numerically predicted three-dimensional turbulent flow and heat transfer for rotating two-pass smooth rectangular channels. They investigated the effect of rotation, channel orientation and the effect of a sharp 180-degree bend on velocity and temperature distributions. They employed a multi-block Reynolds-Averaged Navier-Stokes (RANS) method in conjunction with a near-wall second-moment turbulence closure. Their results well predicted the complex three-dimensional flow and thermal characteristics. Nakayama *et al.* (2003) performed experiments on 180-degree bends and located separated zones and Reynolds stresses. Bansal and Wang (2004) simulated choked refrigerant flow in adiabatic capillary tubes. Koutsou *et al.* (2007) performed Direct Numerical Simulations (DNS) on flow in spacer-filled channels and investigated the impact of spacer dimensions.

*Associate Professor, Dept. of Civil Engineering, University of Maragheh, Maragheh, Iran (E-mail: Daneshfaraz@Maragheh.ac.ir)
**Young Researchers and Elite Club, Maragdeh Branch, Islamic Azad University, Maragheh, Iran (E-mail:alijoudi66@gmail.com)
***Professor, School of Engineering, University of St. Thomas, St Paul, MN, USA (Corresponding Author, E-mail: jpabraham@stthomas.edu)

A series of studies (Sparrow *et al*., 2009; Rend *et al.*, 2013; Abraham *et al*., 2010) numerically simulated flow in diffusers and focused on the impact of divergence angle and flow characteristics on separation, pressure loss, and transition to turbulence. Those studies spanned a wide-range of Reynolds numbers. Sadeghfam and Akhtari (2012) numerically quantified the length and size of a separation zone after a sudden change in direction in closed pipe flows. Daneshfaraz (2013) simulated the flow patterns in a pressurized 90-degree bend and calculated the velocity profile and pressure distribution in bends with various diversion angles. Shokouhmand and Zareh (2014) used both numerical simulation and experimentation to investigate choked refrigerant flow through helical adiabatic capillary tubes. Gorman *et al.* (2011) accurately simulated flow in helical tubes with multiple fluid heat exchange; these flows are similar to the present case in that secondary flows are created which complicate the friction and heat transfer performance. Finally, Kamel *et al.* (2014) used numerical simulation to calculate velocity profiles in open channels with complex geometries.

Despite this rich history of investigation, there is a clear lack of knowledge regarding the performance of different hydraulic structures and the behavior of flow through these structures particularly the bend with a sudden orifice-like constriction. These structures cause many problems with respect to hydraulic performance and maintenance which result in increased cost. To the best knowledge of the authors, there are no studies on the investigation of flow behavior in these structures. Consequently, the aim of this study is to numerically calculate flow velocity profile and pressure variation in the pipe-bend with sudden contraction.

Recent studies have evaluated various turbulence models in swirling/bending flows (Bui, 2008; Galvan *et al.,* 2008) and on particle-laden flows in pipes (Manzar and Shah, 2009; Messa and Malavasi, 2014); compared numerical and experimental curved flows (Sanchez-Silva *et al*., 2003) and simulated vortex flow in large spaces (Sarkardeh *et al*., 2014). In some instances, for example (Bengoechea *et al*., 2014) geometrical parameters of a flow scenario were varied when a swirl was induced in the fluid. While these studies have not directly examined the problem under consideration here, they provide guidance for both numerical analyses and the experimental comparisons carried out here.

One outcome of the present work is that it provides information which can allow a practicing fluid engineer to predict *a priori* the hydraulic impact of a constricted bend on a larger fluid conveyance system (in a way similar to commonly encountered minor loss coefficients that are used to characterize values, bends, expansions, contractions, etc). Finally, this study will investigate the local behavior of the flow (through the pressure and the velocity) for various Reynolds numbers and constrictions.

2. Materials and Methods

2.1 Governing Equations

The governing equations of fluid flow (Navier-Stokes equations) are nonlinear differential equations that describe fluid motion based on conservation of mass and momentum. The equations, which can be found in many fluid mechanics texts, such as Batchelor (1967) can be written in vector form as:

$$\rho\left(\frac{\partial \vec{V}}{\partial t}+\vec{V}\cdot\nabla\vec{V}\right)=-\nabla p+\nabla\cdot\vec{T}+\vec{f} \tag{1}$$

In Eq. (1), V is the fluid velocity, ρ is the density, p is the pressure, T is the local shear stress, and f represents the volumetric body forces on the fluid. Eq. (1) is based on the assumption of incompressible flow and it can be further simplified for Newtonian fluids so that

$$\rho\left(\frac{\partial \vec{V}}{\partial t}+\vec{V}\cdot\nabla\vec{V}\right)=-\nabla p+\mu\nabla^2\vec{V}+\vec{f} \tag{2}$$

where μ is the dynamic viscosity (Acheson, 1990).

The terms in Eq. (2), from left to right, represent the inertial term, convective acceleration, pressure gradient, shear stress, and body force terms. For a steady flow in a cartesian (x, y, z) coordinate system where the respective velocities are u, v, and w, Eq. (2) can be rewritten as

$$\rho\left(u\frac{\partial u}{\partial x}+v\frac{\partial u}{\partial y}+w\frac{\partial u}{\partial z}\right)=-\frac{\partial P}{\partial x}+\mu\left(u\frac{\partial^2 u}{\partial x^2}+v\frac{\partial^2 u}{\partial y^2}+w\frac{\partial^2 u}{\partial z^2}\right) \tag{3}$$

$$\rho\left(u\frac{\partial v}{\partial x}+v\frac{\partial v}{\partial y}+w\frac{\partial v}{\partial z}\right)=-\frac{\partial P}{\partial y}+\mu\left(u\frac{\partial^2 v}{\partial x^2}+v\frac{\partial^2 v}{\partial y^2}+w\frac{\partial^2 v}{\partial z^2}\right) \tag{4}$$

$$\rho\left(u\frac{\partial w}{\partial x}+v\frac{\partial w}{\partial y}+w\frac{\partial w}{\partial z}\right)=-\frac{\partial P}{\partial z}+\mu\left(u\frac{\partial^2 w}{\partial x^2}+v\frac{\partial^2 w}{\partial y^2}+w\frac{\partial^2 w}{\partial z^2}\right) \tag{5}$$

These three momentum equations are combined with the continuity equation of

$$\frac{\partial u}{\partial x}+\frac{\partial v}{\partial y}+\frac{\partial w}{\partial z}=0 \tag{6}$$

The three velocity components are obtained by simultaneously solving Eqs. (3)-(6). With the finite-volume method; integration of these equations is performed over a multitude of small control volumes which constitute the fluid region. The result of the discrete integration is a system of algebraic equations which is then solved by iteration. The iteration process is continued until an appropriate level of accuracy is obtained.

For flow that is laminar, the viscosity is taken to be the molecular viscosity of the fluid. For turbulent flow, the viscosity is a combination of the molecular and the turbulent viscosities from a Reynolds-Averaged Navier Stokes (RANS) model which will now be discussed.

The solution of the discretized Navier-Stokes equations was facilitated by control-volume analysis on each computational element. The solution to the pressure equation was obtained using the Standard scheme for separating the displacement terms in the momentum and turbulence equations. For turbulence transport, an upwind scheme was used and the SIMPLE pressure-

velocity coupling was employed. The turbulence was dealt with using the κ-ε RNG turbulence model. This turbulence model is a modification of the standard κ-ε model from Launder and Spalding (1974). It was perhaps first articulated by Yakhot *et al*. (1992). Its selection here is motivated by its improved ability to handle flows with rotation. The κ-ε RNG turbulence model is expressed mathematically by the two transport equations for the dependent variables κ and ε which represent, respectively, turbulence kinetic energy and turbulent dissipation. While the results presented in the following all correspond to this selected turbulence model, a comparison with a different turbulence model will be given later to demonstrate the independence of the selected model.

$$\frac{\partial(\rho k u_i)}{\partial x_i} = \frac{\partial\left(\alpha_k \mu_{eff} \frac{\partial \kappa}{\partial x_j}\right)}{\partial x_j} + G_k + G_b - \rho\varepsilon + S_k \tag{7}$$

and

$$\frac{\partial(\rho \varepsilon u_i)}{\partial x_i} = \frac{\partial\left(\alpha_k \mu_{eff} \frac{\partial \varepsilon}{\partial x_j}\right)}{\partial x_j} + C_{1\varepsilon}\frac{\varepsilon}{k}(G_k + C_{3\varepsilon}G_b) - \rho C_{3\varepsilon}\frac{\varepsilon^2}{k} - R + S_\varepsilon \tag{8}$$

Here, tensor notation is used for brevity. The *G* terms represent turbulent production from various sources as indicated by the subscripts. The terms *S* correspond to source productions which may exist in the flow. The α terms are inverse Prandtl numbers.

The outcome of Eqs. (7) and (8) is a turbulent component of the viscosity which is added to the molecular viscosity in Eqs. (3)-(5).

The fluid chosen for the simulation was water in the temperature of 20°C and the values of density and dynamic viscosity are 1000 kg/m^3 and 0.001003 kg/m-s, respectively. Since the results are presented in dimensionless format, the Reynolds number can be changed by changing the velocity or fluid properties, the final results will only depend on the Reynolds number.

2.2 Model Geometry, Meshing and Boundary Conditions

In this study, the flow in a 90-degree bend is simulated using commercially available software (FLUENT). The primary aim of this study is to investigate the effect of a flow constriction on the velocity profile and pressure variation. The first stage of the simulation was a calculation of these parameters (velocity and pressure) in the absence of a constriction and at a Reynolds number of 300 to validate the simulations with the experimental results of Olsen (1971). The radius of curvature was identical to that of Olson (1971) and is equal to 24 mm.

The inlet and outlet legs of the bend extended upstream and downstream 300 mm and 150 mm, respectively. The diameter of the pipe was 8 mm. The legs are sufficiently long to allow for sufficient development of the flow (Kays and Crawford, 1993; Abraham *et al*., 2008; Abraham *et al*., 2009; Abraham *et al*., 2011). Much of the analysis that follows will be presented in a dimensionless format. In addition, following the initial low Reynolds calculations, the analysis was extended to larger Reynolds flows and to flows that are turbulent. The values of

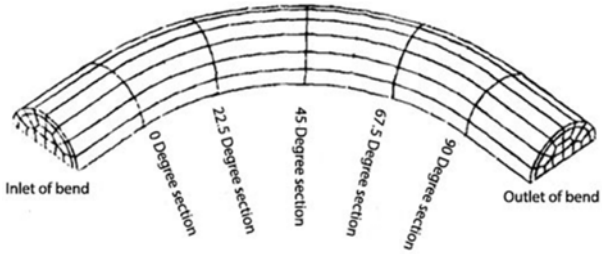

Fig. 1. Schematic of the Pipe Bend, with Annotation Showing Locations Used for Data Extraction

investigated Reynolds numbers were 100, 500, 850, 4800, and 10000.

Constrictions which blocked 20%, 40%, and 60% of the cross section were studied. These constrictions were placed at the upstream end of the bend. A locating scheme was used wherein the arc angle (from 0° to 90°) defined the position along the bend. Discrete values of 0, 22.5, 45, 67.5, and 90 are used. Fig. 1 has been prepared to provide a visual description of the geometry of the bend.

The effects of gravity are not included in the analysis because of the small dimensions of the pipe and the dominating effects of momentum and friction.

Next, a series of images are provided to display the contraction which is positioned at the upstream end of the bend. In the first image (Fig. 2) a 20% contraction is shown. The subsequent figures correspond to the 40% and 60% obstructions.

2.3 Boundary Conditions

Boundary conditions are required at all boundaries of the fluid

Fig. 2. A 20% Obstruction Placed at the Leading Edge of the Bend

Fig. 3. A 40% Obstruction Placed at the Leading Edge of the Bend

Fig. 4. A 60% Obstruction Placed at the Leading Edge of the Bend

region. The conditions are placed at the inlet, outlet, wall-fluid interface, and on the symmetry plane of the pipe because these situations have been shown both experimentally and numerically to have two symmetric secondary flows in the two halves of the channels. At the inlet, a specified velocity was assigned. At the outlet, a pressure was given and zero second derivatives were asserted on all transported variables. At the wall-fluid interface, a no-slip condition is used. Wall functions were used to span the viscous sub layer in the turbulent calculations. At the inlet, the turbulence intensity for flows whose Reynolds numbers were in the turbulence regime were set by the following correlation.

$$Turbulent\ Intensity = 0.16Re^{-\left(\frac{1}{8}\right)} \quad (9)$$

2.4 The Computational Mesh

The solution domain was discretized into a computational mesh using commercially available software (Gambit) which is useful for obtaining block and hexahedral elements. Fig. 5 shows the mesh near the bend region and a close-up view of the mesh near the obstruction is provided. The close-up shows the reduction of element size adjacent to the obstruction.

The four investigated cases required different element numbers for the various geometries. A summary listing is provided in Table 1. It is expected and seen that the greater constrictions required a larger number of elements. The results to be presented here were subjected to a mesh-independence verification wherein the computational mesh was refined and the key results (pressure and velocity values) were found to be independent of the mesh.

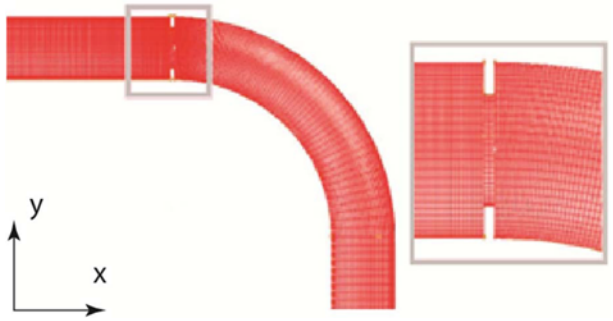

Fig. 5. Image of the Computational Mesh with a Focused View on the area Adjacent to the Constriction

Table 1. Amount of Meshing in Different Levels of Contraction

Number of hexahedron elements	Case
115141	No Contraction
138200	% 20
155104	% 40
170944	% 60

For each calculation, the iteration process was continued until the transported variables met a convergence requirement of 0.0001 for their residuals. 250-300 iterations were required for this level of convergence.

2.5 The Numerical Solution and Validation

As stated earlier, the solution of the discretized Navier-Stokes equations was facilitated by control-volume analysis on each computational element. The solution to the pressure equation was obtained using the Standard scheme for separating the displacement terms in the momentum and turbulence equations. For turbulence transport, an upwind scheme was used and the SIMPLE pressure-velocity coupling was employed.

The turbulence was dealt with using the κ-ε RNG turbulence model. The selection of a κ-ε based turbulence model was made in part because of this models long and successful history modeling internal wall-bounded flows. The κ-ε model was the first two-equation turbulence model to be developed approximately 45 years ago. In the subsequent years, numerous variants of this model have appeared (like the Renormalized Group technique, RNG). Furthermore, other Reynold-Averaged Navier Stokes approaches using one, two, or more transport equations have been developed. More recent methods such as direct numerical simulation or large eddy simulation are coming into use now however the computational resources required for these newer approaches are prohibitively expensive in most cases. So here, the selection of the turbulence model was based on its successful history for these types of flows and the balance it possesses between accuracy and required computational resources. A discussion will be provided later in this manuscript related to the accuracy of the turbulence model and the sensitivity of the results because of model selection.

A comparison of the results with experimental data is provided in Fig. 6; both the simulations and experiments corresponded to a Reynolds number of 300. In the figure (and in following figures), values of the abscissa are measured from the inner surface to the outer surfaces in the radial direction. The experiments, taken from Olson (1971) are nearly indistinguishable from the calculations. The sequence of figures show velocity profiles extracted at a series of axial locations as indicated by the caption. It is seen that at the most upstream location, the velocity profile is axisymmetric across the cross section. At progressively more downstream locations, the flow is predisposed to a non-symmetric profile with a progressively larger peak flow moving outward in the radial direction. At each of these streamwise locations, the

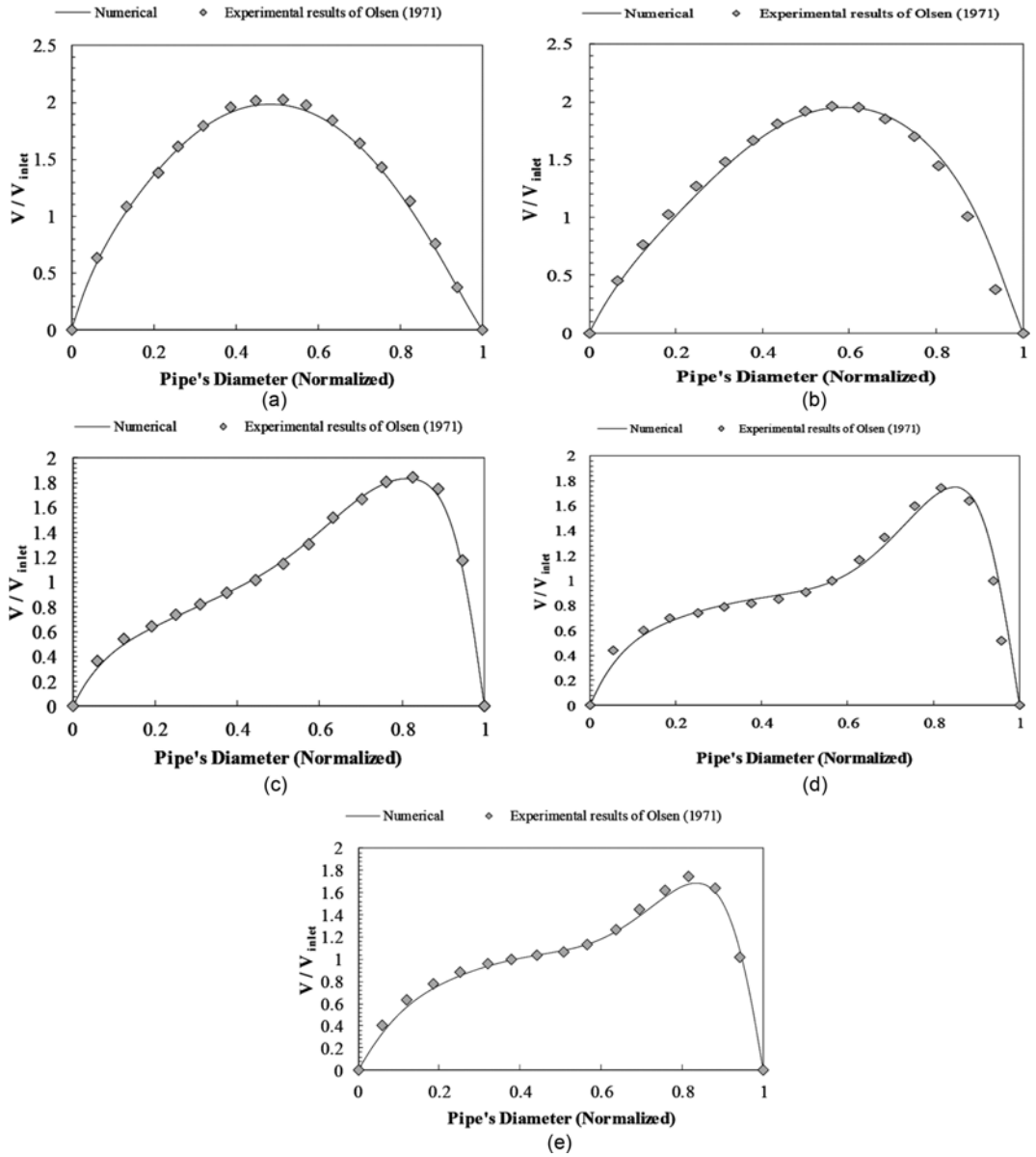

Fig. 6. The Profile of Velocity for 90 degree Bend in Different Sections in Comparison with Results of Olson (1971) (a) 0 degrees, (b) 22.5 degrees, (c) 45 degrees, (d) 67.5 degrees, (e) 90 degrees

numerical simulations and experiments agree not only qualitatively (shape of the curve) but also quantitatively (local values of velocity).

The experimental results of Olson were obtained with a Perspex tube with an internal radius of 4 mm (diameter of 8 mm) and a curvature radius of 24 mm (same as the simulation). The tube wall was transparent and local velocity measurements were obtained using laser-Doppler anemometry.

Next, the results for other Reynolds numbers are shown (ranging from 100 to 10,000). This range of Reynolds numbers covers many of the practical flow scenarios encountered in practice. At the lower end of this range, the flow is deeply laminar so no new flow phenomena are expected for even more laminar flow. At the upper end of this range, the flow is fully turbulent so that all of the major turbulent behaviors will be manifest. In fact, it will be seen that that flow results become self-similar for the larger Reynolds number situations. Figs. 7-10 show a progression of constrictions; each image shows velocity profiles at five stream wise locations.

In Figs. 7(a) and (b), comparisons between a very low and higher Reynolds number are made. It is seen that the higher Reynolds number flow results in a stronger predisposition of flow toward the outer surface of the pipe. At the lower Reynolds number (Re = 100), the general shape of the previously axisymmetric shape is maintained with an outward shift in the peak of the velocity profile.

Next, Fig. 8 displays two cases for the 20% constriction situation. It should be noted that the Reynolds numbers in Fig.8

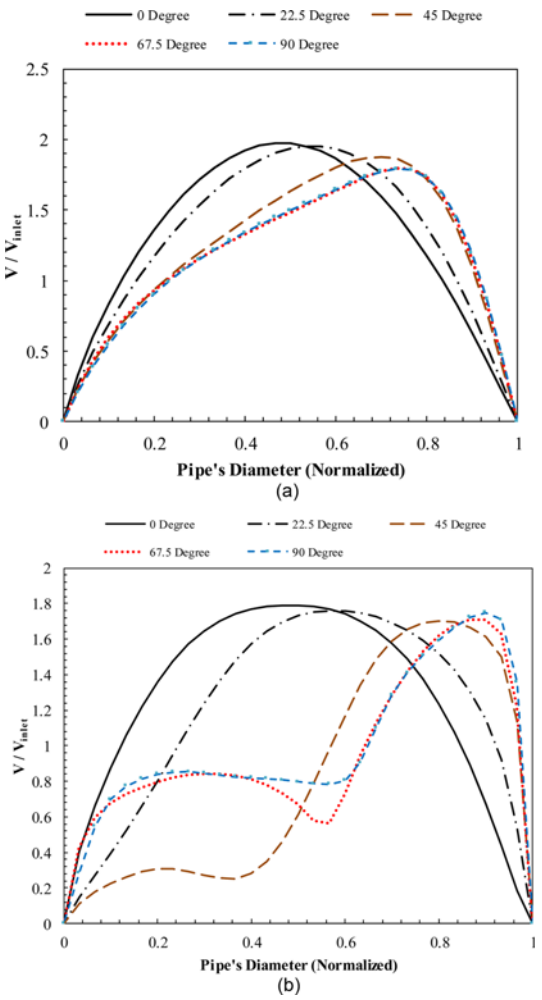

Fig. 7. Velocity Profile for 90 degree Bend in Different Sections without a Constriction: (a) Reynolds Number Equals 100, (b) Reynolds Number Equals 1800

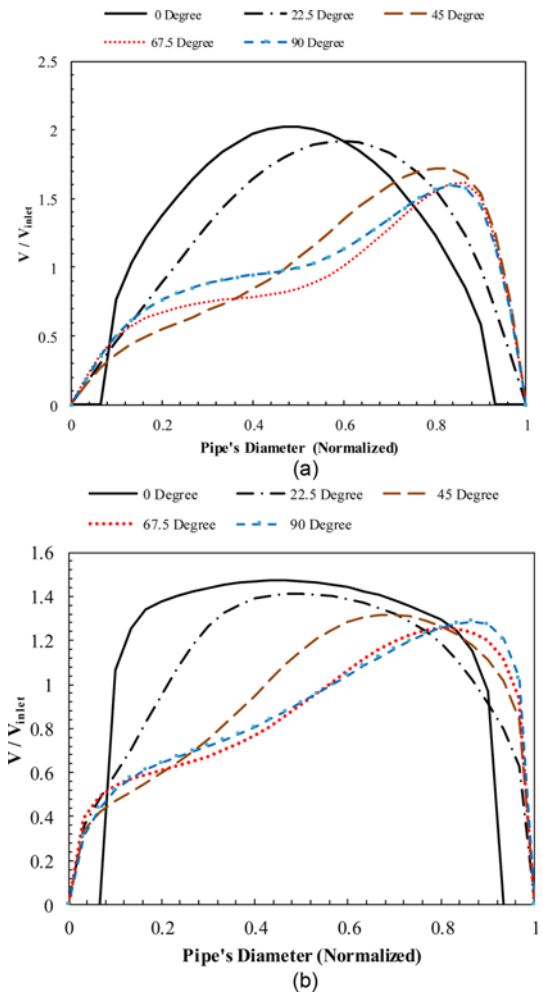

Fig. 8. Velocity Profile for 90 Degree Bend in Different Sections with a Constriction of 20%: (a) Reynolds Number Equals 500, (b) Reynolds Number Equals 4800

are higher than those in Fig. 7. In fact, they enter the turbulent regime. For the higher Reynolds number case, the typical flatter velocity profiles are observed. It is also noted that the downstream normalized velocity profiles are much similar in Fig. 8 when compared with Fig. 7.

Next, Fig. 9 displays results for the next constriction situation (40%) and for higher Reynolds numbers. In this comparison, the (a) figure continues to be laminar whereas the (b) part is deeply turbulent. The resulting profiles are clearly distinctive with a largely parabolic laminar profile for the (a) part and a characteristic turbulent profile for the (b) image. What is noteworthy is that despite these very different turbulence states, the normalized velocity profiles are not very different at the downstream locations. It is also noted that as the contraction increases (Fig. 9 compared with Fig. 8), it is seen that the downstream flow is more predisposed toward the outer wall.

The trends from the prior figures continue in Fig. 10. Here, the constriction is a maximum (60%) and the higher Reynolds number is deeply turbulent. Again the turbulent profile is seen at the upstream locations while at the downstream locations, the flow is strongly forced outwards; a trend that extends that from the prior figures. This finding is rationalized by recognizing that flow passing through a contraction emerges as a jet-like flow with a higher momentum than would otherwise occur if no contraction had been present. This jet-like flow with its larger momentum is compressed to the outer wall and is unable to follow the contour of the inner radius.

The results show that with increasing Reynolds number, the flow is forced towards the outer bend of the pipe. There is a tendency toward separation in the more downstream cross sections (45 and 67.5° locations), particularly for the more severe constriction cases.

Next, Fig. 11 is provided to show the cross sectional peak velocities. The figures are arranged by increasing constriction and are normalized to the cross-sectional average velocity. It is seen that the values of the peak velocity depend on Reynolds number, particular for flows that are clearly laminar or clearly turbulent. We find non-constricted peak velocities of approximately

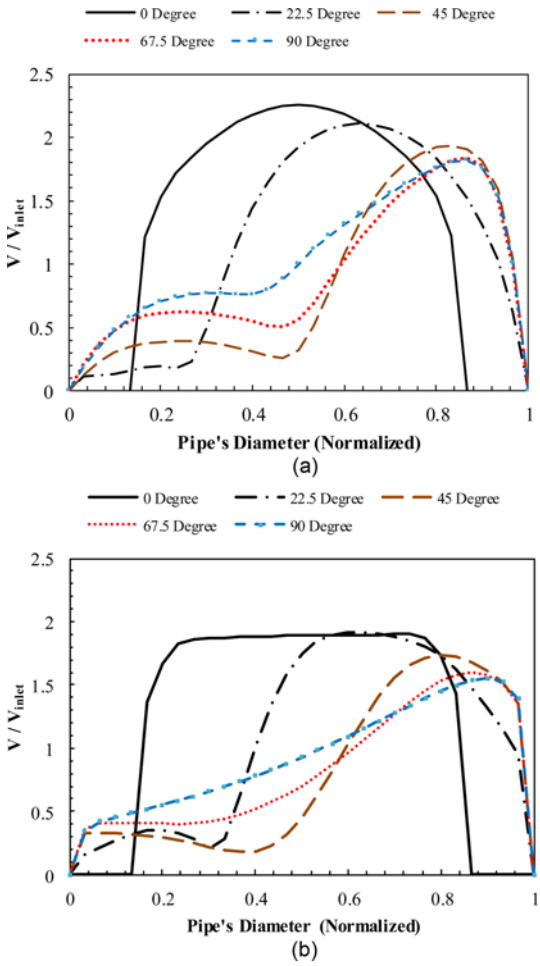

Fig. 9. Velocity Profile for 90 Degree Bend in Different Sections with a Constriction of 40%: (a) Reynolds Number Equals 850, (b) Reynolds Number Equals 10000

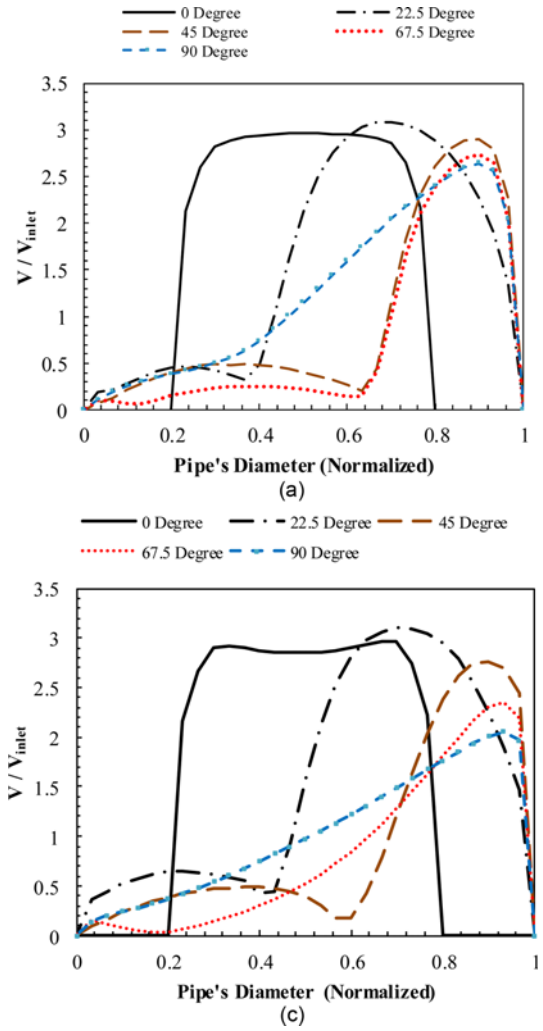

Fig. 10. Velocity Profile for 90 Degree Bend in Different Sections with a Constriction of 60%: (a) Reynolds Number Equals 1800, (b) Reynolds Number Equals 10000

2 for the most laminar cases and a peak velocity of approximately 1.25 for the turbulent situation. These findings agree with expected solutions for fully developed laminar and turbulent profiles in round tubes.

For the cases with a constriction, it is seen that the peak velocities increase and the range decreases. At the most extreme constriction of 60%, the peak velocities at the most upstream location is 3 for all cases and it decreases to values in the range of 2-2.5 at the most downstream location.

Finally, Fig. 12 gives a comparison of the relative pressure decrease for the various cases. The pressure drop at each axial location is related to the pressure at the inlet (just downstream of the orifice) and is made dimensionless by the dynamic pressure. The definition of the pressure decrease is

$$\Delta P = \frac{P - P_{inlet}}{\frac{1}{2}\rho \overline{V}^2} \tag{10}$$

where $\overline{V}$ is the cross-sectional average velocity.

It is seen that first, particularly for the lesser obstructed cases, lower Reynolds numbers lead to a nearly linear pressure decrease. It is generally expected that the pressure will decrease as the flow passes through the elbow but the pattern of decrease may differ depending on the situation.

From Fig. 12, it is seen that as Reynolds numbers increase, the pressure drop becomes more nonlinear and converges to a value as the Reynolds number continues to increase. This finding is seen in all of the Fig. 12 images and for all obstructions. These findings show a clear dependence of the pressure loss to Reynolds number. A quick review of the images reveals that for the lower Reynolds number case, the pressure does, in fact, decrease in the flow direction. As the Reynolds number increases the pressure drop tends to occur in the first part of the bend and pressures are more constant thereafter. This finding reflects the fact that for higher Reynolds number, the pressure losses are more closely related to contraction/expansion losses and less so to friction. In fact, in some cases, there is a partial pressure recovery downstream of the contraction as the flow expands and slows.

It is also seen that there is a great consistency between the various blockage cases at low Reynolds numbers however as

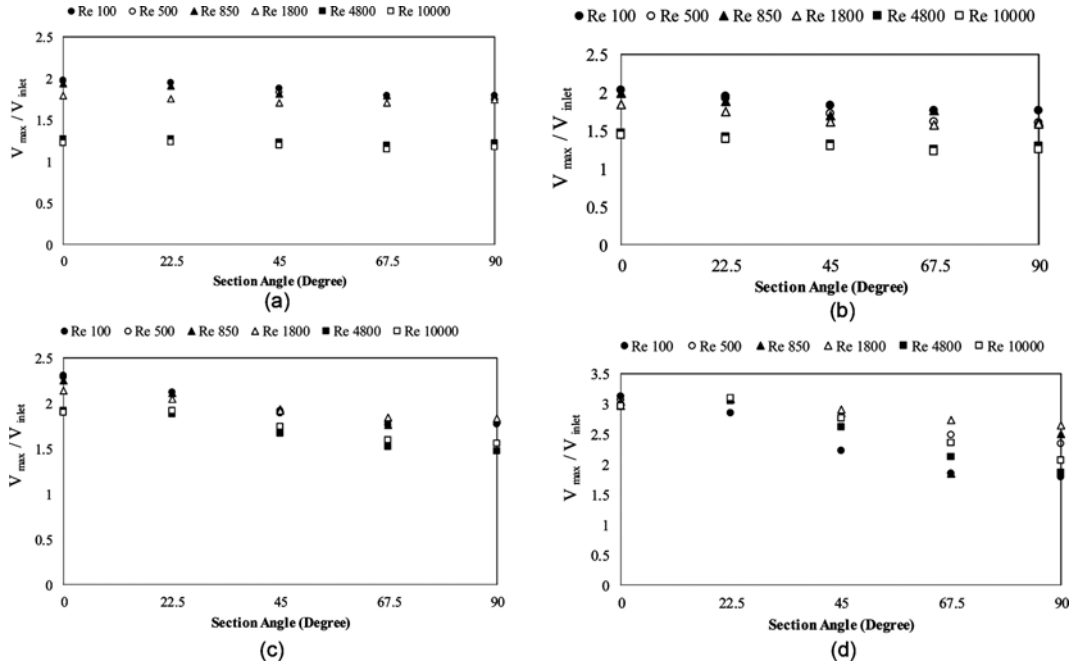

Fig. 11. Relative Maximum Velocity of Bend: (a) Without a Constriction, (b) 20% Constriction, (c) 40% Constriction, (d) 60% Constriction

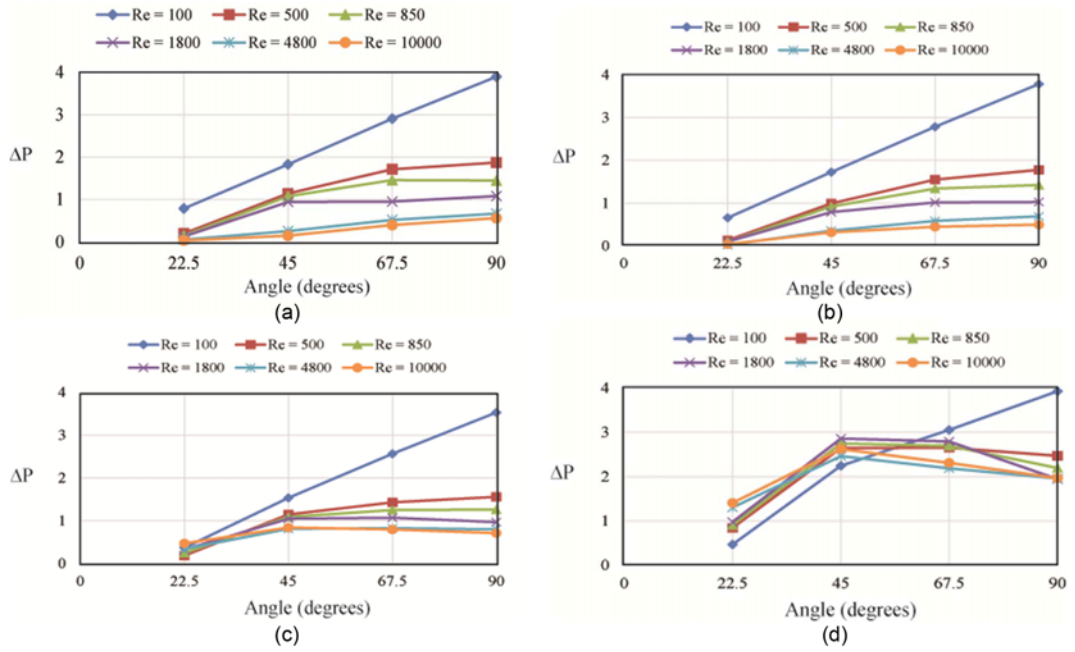

Fig. 12. Relative Pressure Drop for Bend with: (a) No Constriction, (b) with a Constriction of 20%, (c) with Constriction of 40%, (d) with Constriction of 60%

Reynolds numbers increase the different orifices lead to increasingly different pressure loss values.

It is also seen that the results are in agreement with the literature for pressure losses in 90-degree bends although the wide spread in reported literature make an exact comparison impossible, the results presented here are bounded by the prior work (Crane, 1999).

While the results of the calculation are shown to agree well with prior work and with authoritative engineering technical manuals, care should be noted for the limitations. These results pertain to the specific Reynolds number and location of the contraction in the bend. For cases where the constriction is located elsewhere (either further upstream, further downstream, or non-axisymmetric, new analyses would be required. In addition, for the case studied here, the flow was assumed to enter into the system flowing in a uniform and axially directed manner. If there

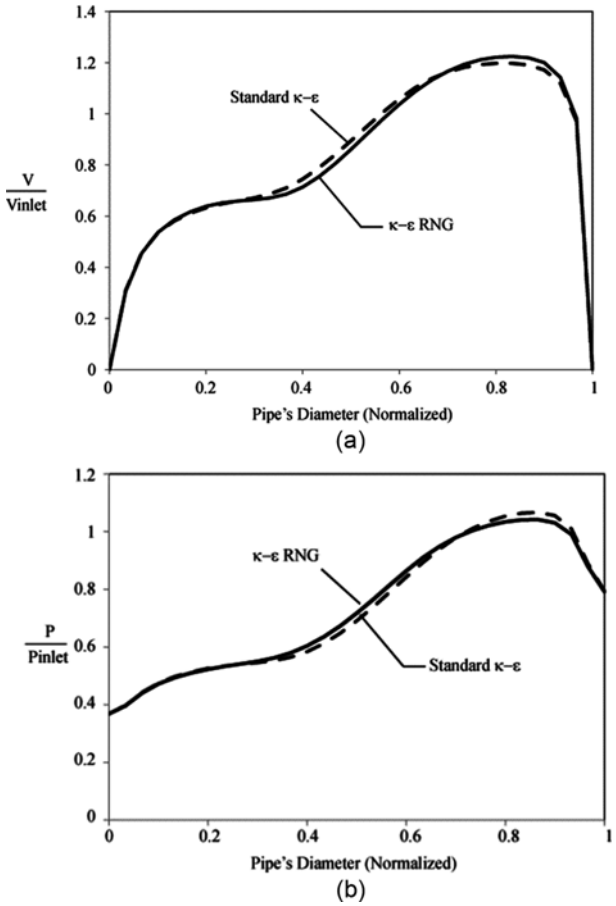

Fig. 13. Comparison of: (a) Velocity Profiles, (b) Pressure Variations Across the Cross Section at the Exiting Plane of the Bend for Two Different Turbulence Models and for a Reynolds Number of 10,000 and no Constriction

are other piping structures upstream of the bend, the flow would enter with some already formed predisposition and this predisposition would have to be incorporated into further study.

2.6 Sensitivity of Selected Turbulence Model

In order to test the influence of the chosen turbulence model, a second calculation was completed using the standard κ-ε model from Launder and Spalding (1974). Figs. 13(a) and (b) show normalized velocity and pressure distributions across the cross section at the downstream end of the bend (90 degree location) for the non-contraction case and for Re = 10,000. It is seen that both pressure and velocity distributions are nearly identical. The results shown in Figs. 13(a) and (b) are representative. Comparisons of other locations and contraction cases showed similar excellent agreement which strongly suggests the results are not dependent on the specific details of the selected turbulence model.

3. Conclusions

In this study, a numerical simulation model was used to characterize fliud flow in a 90-bend with an upstream constriction. The calculations spanned Reynolds numbers from 100 to 10,000. Simulations in the turbulent regime was accomplished using a κ-ε RNG turbulence model. Results for the unconstructed case were compared with experimental findings in the literature and found to be in excellent agreement.

The results included the no constriction case and constrictions that blocked 20%, 40%, and 60% of the flow area. It was seen that the presence of the constriction had a notable impact on the velocity profiles and predisposed flow toward the outer bend of the pipe. There was a tendency of the velocity to be more prone to separation, particularly at locations of 45° and 67.5°. Calculations of the maximum velocity were also made and for the no contraction case, the results agreed very well with expected laminar and turbulent profiles. As the constriction became more severe, larger values of the peak velocity were found and the dependence on Reynolds number was reduced. Independent of the Reynolds number, as the flow progressed through the bend, the maximum velocity decreased.

With respect to pressure, it was found that some cases (large Reynolds number and significant constrictions) experienced negative pressures. And that there were locally large pressure drops for the larger flowrates and more severe constriction. The results here can be interpreted as archival pressure loss results for future fluid flow calculations.

References

Abraham, J. P., Sparrow, E. M., and Minkowycz, W. J. (2011). "Internal-flow Nusselt numbers for the low-Reynolds number end of the laminar-to-turbulent transition regime." *Int. J. Heat Mass Transfer,* Vol. 54, Nos. 1-3, pp. 584-588.

Abraham, J. P., Sparrow, E. M., Tong J. C. K., and Bettenhausen, D. W. (2010). "Internal flows which transist from turbulent through intermittent to laminar." *Int. J. Thermal Sciences*, Vol. 49, No. 2, pp. 256-263.

Abraham, J. P., Tong, J. C. K., and Sparrow, E. M. (2008). "Breakdown of laminar pipe flow into transitional intermittency and subsequent attainment of fully developed intermittent or turbulent flow." *Num. Heat Transfer B*, Vol. 54, No. 2, pp. 103-115.

Abraham, J. P., Tong, J. C. K., and Sparrow, E. M. (2009). "Heat transfer in all pipe flow regimes – laminar, transitional/intermittent, and turbulent." *Int. J. Heat Mass Transfer*, Vol. 52, Nos. 3-4, pp. 557-563.

Acheson, D. J. (1990). *Elementary Fluid Dynamics*, Oxford Applied Mathematics and Computing Science Series. New York: Oxford University Press.

Al-Qahtani, M., Jang, Y., Chen, H., and Han, J. (2002). "Flow and heat transfer in rotating two-pass rectangular Channels (AR=2) by Reynolds stress turbulence model." *Int. J. Heat Mass Transfer*., Vol. 45, No. 9, pp. 1823-1838.

Bansal, P. K. and Wang, G. (2004). "Numerical analysis of choked refrigerant flow in adiabatic capillary tubes." *Appl. Therm. Eng*., Vol. 24, Nos. 5-6, pp. 851-863.

Batchelor, G. K. (1967). *An Introduction to Fluid Dynamics*, London: Cambridge University Press.

Bengoechea, A., Anton, R., Larraona, G. S., Ramos, J. C., and Rivas, A. (2014) "Influence of geometrical parameters on downstream flow of a screen under fan-induced swirl." *Conditions Eng. Appl. Comp.*

Fluid Mech., Vol. 8, No. 4, pp. 623-638.

Bovendeerd, P. H. M., Steenhoven, A. A. V., Vosse, F. N. V. D., and Vossers, G. (1987). "Steady entry flow in a curved pipe." *J. Fluid Mech*., Vol. 177, pp. 233-246.

Bui, V. A. (2008) "Simplified turbulence models for confined swirling flows." *Eng. Appl. Comp. Fluid Mech*., Vol. 2, No. 4, pp. 404-410.

Crane (1999). "Flow of Fluids Through Valves, Fittings, and Pipes." Crane Valves North American, Technical Paper No. 410M, 1999.

Daneshfaraz, R. (2013). "3-D Investigation of velocity profile and pressure distribution in bends with different diversion angle." *Journal. Civil Eng. Sci*., Vol. 2, No. 4, pp. 234-240.

Galvan, S., Reggio, M., and Francois, G. (2011). "Assessment study of k-e turbulence models and near-wall modeling for steady state swirl analysis in drift tube using Fluid." *Eng. Appl. Comp. Fluid Mech.,* Vol. 5, No. 4, pp. 459-478.

Gorman, J. M., Sparrow, E. M., Mowry, G. S., and Abraham, J. P. (2011). "Simulation of helically wrapped, compact heat exchangers." *J. Renew. Sustain. Energy*, 3, article no. 043120.

Kamel, B., Kriba, I., Ali, F., and Abdelbaki, D. (2014). "3D simulation of velocity profile of turbulent flow in open channel with complex geometry." *Phys. Procedia*., Vol. 55, No. 1, pp. 119-128.

Kays, W. M. and Crawford, M. E. (1993). *Convective Heat and Mass Transfer*, McGraw-Hill, New York.

Koutsou, C. P., Yiantsios, S. G., and Karabelas, A. J. (2007). "Direct numerical simulation of flow in spacer-filled channels: Effect of spacer geometrical characteristics." *J. Membrane. Sci*., Vol. 291, Nos. 1-2, pp. 53-69.

Launder, B. E. and Spalding, D. B. (1974). "The numerical computation of turbulent flows." *Comp. Method. Appl. Mech. Eng.,* Vol. 3, No. 2, pp. 269-289.

Manzar, M. A. and Shah, S. N. (2009). "Particle distribution and erosion during the flow of Newtonian and non-Newtonian slurries in straight and coiled pipes." *Eng. Appl. Comp. Fluid Mech*., Vol. 3, No. 3, pp. 296-320.

Messa, G. V. and Malavasi, S. (2014). "Numerical prediction of particle distribution of solid-liquid slurries in straight pipes and bends." *Eng. Appl. Comp Fluid Mech*., Vol. 8, No. 3, pp. 356-372.

Morrissey, M. M. and Chouet, B. A. (1997). "A numerical investigation of choked flow dynamics and its application to the triggering mechanism of long-period events at Redoubt Volcano, Alaska." *J. Geophys. Res.*, Vol. 102, No. B4, pp. 7965-7983.

Nakayama, H., Hirota, M., Fujita, H., Yamada, T., and Koide, Y. (2003). "Flow characteristics in rectangular ducts with a sharp 180-degree turn." *JSME*, Vol. 2, No. 1028, pp. 1171-1179.

Olson D. E. (1971). *Fluid mechanics relevant to respiration: Flow within curved or elliptical tubes and bifurcating systems*, Ph.D. Thesis, University of London.

Rend, R. R., Sparrow, E. M., Bettenhausen, D. W., and Abraham, J. P. (2013). "Parasitic pressure losses in diffusers and in their downstream piping systems for fluid flow and heat transfer." *International Journal of Heat and Mass Transfer*, Vol. 61, No. 1, pp. 56-61.

Sadeghfam, S. and Akhtari, A. A. (2012). "Numerical investigation of length and thickness of separation zone after sudden change of direction in closed Sections." *Journal. Civil Eng. Urban*., Vol. 2, No. 1, 35-39.

Sanchez-Silva, F., Gomer, A., Toledo, M., Quinto, P., and Zurita, V. (2003). "Experimental and numerical curved flow study for metrology purposes." *J. Appl. Res. Tech.,* Vol. 1, No. 2, pp. 114-126.

Sarkardeh, H., Zarrati, A.R., Jabbari, E., and Marosi, M. (2014). "Numerical simulation and analysis of flow in a reservoir in the presence of vortex." *Eng. Appl. Comp. Fluid Mech*., Vol. 8, No. 4, pp. 598-608.

Shokouhmand, H. and Zareh, M. (2014). "Experimental investigation and numerical simulation of choked refrigerant flow through helical adiabatic capillary tube." *Appl. Therm. Eng*., Vol. 63, No. 1, pp. 119-128.

Sparrow, E. M., Abraham, J. P., and Minkowycz, W. J. (2009). "Flow separation in a diverging conical duct: Effect of Reynolds number and divergence angle." *Int. J. Heat Mass Transfer*, Vol. 52, Nos. 13-14, pp. 3079-3083.

Van De Vosse, F. N., Van Steenhoven, A. A., Segal, A., and Janseen, J. D. (1989). "A finite element analysis of steady laminar entrance flow in a 90 Curved tube." *Int. J. Numer. Meth. F.*, Vol. 9, No. 3, pp. 275-287.

Yakhot, V., Orszag, S. A., Thangam, S., Gatski, T. B., and Speziale, C. G. (1992). "Development of turbulence models for shear flows by a double expansion technique." *Phys. Fluids A,* Vol. 4, No. 7, pp. 1510-1520.